

## RESEARCH REPORT

# The ETS transcription factor Spi2 regulates hematopoietic cell development in zebrafish

Shizheng Zhao<sup>1,\*</sup>, Ao Zhang<sup>1,\*</sup>, Hao Zhu<sup>1</sup> and Zilong Wen<sup>1,2,‡</sup>

## ABSTRACT

The E26 transformation-specific or E-twenty-six (ETS) genes encode a superfamily of transcription factors involved in diverse biological processes. Here, we report the identification and characterization of a previously unidentified member of the ETS transcription factors, Spi2, that is found exclusively in the ray-finned fish kingdom. We show that the expression of *spi2* is restricted to hemogenic endothelial cells (HECs) and to hematopoietic stem and progenitor cells (HSPCs) in zebrafish. Using bacteria artificial chromosome transgenesis, we generate a *spi2* reporter line, *TgBAC(spi2:P2a-GFP)*, which manifests the GFP pattern recapitulating the endogenous *spi2* expression. Genetic ablation of *spi2* has little effect on HEC formation and the endothelial-to-hematopoietic transition, but results in compromised proliferation of HSPCs in the caudal hematopoietic tissue (CHT) during early development and in severe myeloid lineage defect in adulthood. Epistatic analysis shows that *spi2* acts downstream of *runx1* in regulating HSPC development in the CHT. Our study identifies Spi2 as an essential regulator for definitive hematopoietic cell development and creates a *TgBAC(spi2:P2a-GFP)* reporter line for tracking HECs, HSPCs, myeloid cells and thrombocytes from early development to adulthood.

**KEY WORDS:** Zebrafish, Hematopoiesis, Hematopoietic stem/progenitor cells, ETS transcription factors

## INTRODUCTION

Vertebrate blood development comprises primitive and definitive hematopoiesis, with definitive hematopoiesis generating hematopoietic stem and progenitor cells (HSPCs) capable of self-renewal and differentiation into all hematopoietic lineages (Kondo et al., 2003; Jagannathan-Bogdan and Zon, 2013). The definitive HSPCs arise from hemogenic endothelial cells (HECs) in the floor of the dorsal aorta (DA) in the aorta-gonad-mesonephros (AGM) through endothelial-to-hematopoietic transition (EHT) (Bertrand et al., 2010; Boisset et al., 2010; Kissa and Herbomel, 2010). After emergence from the AGM, HSPCs migrate to the intermediate hematopoietic tissues, the fetal liver in mammals or the caudal hematopoietic tissue (CHT) in zebrafish (Murayama et al., 2006; Jin et al., 2007), and finally colonize the adult hematopoietic tissues,

the bone marrow in mammals or the kidney marrow (KM) in zebrafish (Jagannathan-Bogdan and Zon, 2013).

The E26 transformation-specific or E-twenty-six (ETS) genes encode a superfamily of transcription factors containing a conserved DNA-binding ETS domain (Sharrocks, 2001; Sizemore et al., 2017). In mammals, the ETS family consists of 27–28 members that are involved in many cellular processes, including hematopoiesis (Sizemore et al., 2017). For example, the ETS variant 2 (*Etv2*) is a key regulator for hemogenic angioblast formation and HEC specification (Liu and Patient, 2008; Sumanas and Choi, 2016; Zhao et al., 2022). Likewise, the SPI-subfamily, including PU.1, SPIB and SPIC, are involved in myeloid fate commitment and B cell development (Scott et al., 1994; Su et al., 1997; Kohyama et al., 2009; Willis et al., 2017). In zebrafish, 31 ETS genes have been identified (Liu and Patient, 2008), and some are zebrafish-specific, presumably resulting from a genome duplication event in ray-fin phylogeny (Postlethwait et al., 2000). These duplicated genes may take the partitioning function of the ancestral gene or acquire a new adaptive function (Force et al., 1999). Hence, understanding zebrafish-specific ETS genes may provide evolutionary insights into gene subfunctionalization and neofunctionalization.

In this study, we reported the identification and characterization of a ray-finned fish-specific ETS transcription factor Spi2 and its role in hematopoietic cell development.

## RESULTS AND DISCUSSION

### *spi2* is enriched in HECs and hematopoietic lineages

To investigate the mechanism governing the specification of HECs and conventional endothelial cells (cECs), we have previously isolated HECs and cECs from the floor and roof wall of the DA and performed single cell RNA-sequencing (scRNA-seq) (Zhao et al., 2022). Differentially expressed gene (DEG) analysis revealed that *spi2* was highly expressed in the HECs (Fig. 1A). The Ensembl genome browser showed that *spi2* was found exclusively in ray-finned fishes but not in birds and mammals (Fig. 1B). Phylogenetic tree analysis showed that *spi2* represented a separated evolutionary branch different from other paralogs which have corresponding orthologs in mammals (Fig. 1C). Protein sequence alignment revealed that Spi2 shared 34%~40% similarity with other paralogs in overall protein sequences and 55%~61% similarity in the ETS domain (Fig. 1D; Fig. S1A,B). To confirm the *spi2* expression pattern, we performed whole-mount *in situ* hybridization (WISH). Results showed that *spi2* was first detected in the AGM at ~24 h post-fertilization (hpf) and later was evident in both AGM and CHT at 2 days post-fertilization (dpf) (Fig. 1E; Fig. S1C). Fluorescence *in situ* hybridization (FISH) further confirmed that *spi2* was expressed in 70.0±8.9% (mean±s.d.) of the DA floor *flkl1:GFP*<sup>+</sup> cells at 2 dpf (Fig. 1F,G), where HECs reside (Bertrand et al., 2010; Kissa and Herbomel, 2010; Zhao et al., 2022), and later was also expressed in the subsets (31.2±5.9%)

<sup>1</sup>Division of Life Science, State Key Laboratory of Molecular Neuroscience, Hong Kong University of Science and Technology, Clear Water Bay, Hong Kong, China.

<sup>2</sup>Greater Bay Biomedical Innocenter, Shenzhen Bay Laboratory, Shenzhen Peking University–Hong Kong University of Science and Technology Medical Center, Shenzhen 518055, China.

\*These authors contributed equally to this work

‡Author for correspondence (zilong@ust.hk)

 S.Z., 0000-0002-9859-7559; Z.W., 0000-0002-4260-7682

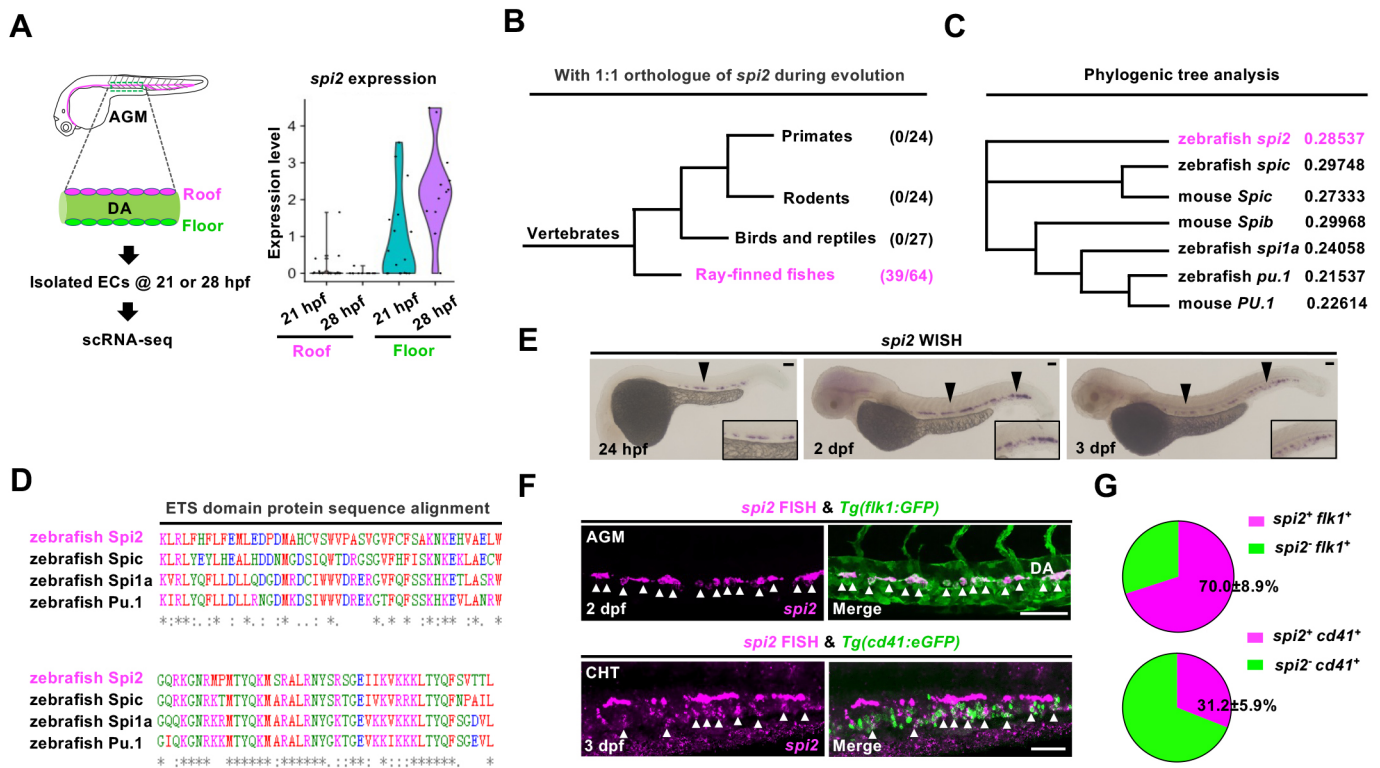


**Fig. 1. Phylogenetic analysis and early expression pattern of *spi2*.** (A) *spi2* expression in the roof and floor of the dorsal aorta (DA) at 21 hpf and 28 hpf by scRNA-seq. ECs, endothelial cells. (B) Analysis of *spi2* gene ortholog (1:1) during vertebrate evolution. Denominator: the number of analyzed species. Numerator: the number of species containing gene ortholog of *spi2*. (C) Phylogenetic tree analysis of SPI-subfamily in zebrafish and mice. (D) Protein sequence alignment of ETS domain among *spi2* paralogs in zebrafish. Asterisks indicate conserved amino acids among *spi2* paralogs. (E) *spi2* WISH at 24 hpf, 2 dpf and 3 dpf. Black arrowheads show *spi2*-expressing cells. (F) *spi2* FISH and anti-GFP antibody staining in the aorta-gonad-mesonephros (AGM) of *Tg(flk1:eGFP)* zebrafish (white arrowheads: *flk1*<sup>+</sup>*spi2*<sup>+</sup> cells) and in the caudal hematopoietic tissue (CHT) of *Tg(cd41:eGFP)* zebrafish (white arrowheads: *cd41*<sup>+</sup>*spi2*<sup>+</sup> cells). (G) Pie chart shows the quantification percentage (±s.d.) of *spi2*<sup>+</sup>*flk1*<sup>+</sup> cells in *flk1*<sup>+</sup> cells in the floor of the DA at 2 dpf (fish *n*=5) or *spi2*<sup>+</sup>*cd41*<sup>+</sup> cells in *cd41*<sup>+</sup> cells in the CHT at 3 dpf (fish *n*=9) in F. Scale bars: 60 μm.

of *cd41:eGFP*<sup>+</sup> cells in the CHT at 3 dpf, which presumably represent definitive HSPCs and thrombocytes (Lin et al., 2005; Bertrand et al., 2008) (Fig. 1F,G). These observations indicate that *spi2* is specifically expressed in HECs and HSPCs during zebrafish early development.

### Generation and characterization of *TgBAC(spi2:P2a-GFP)* reporter line

Given its specific expression pattern, we reasoned that establishing a *spi2* reporter line would provide a useful tool for studying HEC and HSPC emergence. We therefore used bacteria artificial chromosome (BAC) clone CH211-45O10, a 200-kilobase (kb) pairs DNA fragment covering both the upstream and downstream sequences of the *spi2* gene locus, to generate the *spi2* reporter *BAC(spi2:P2a-GFP)* construct by replacing the stop codon with P2a-GFP sequences (Fig. 2A). The *BAC(spi2:P2a-GFP)* constructs were used to generate the *spi2* reporter line. A *TgBAC(spi2:P2a-GFP)* line with stable GFP expression was successfully obtained. To characterize the *TgBAC(spi2:P2a-GFP)* line, we outcrossed it with *Tg(flk1:mCherry)* fish, in which HECs and eECs are labeled by mCherry (Bertrand et al., 2010). Examination of the *TgBAC(spi2:P2a-GFP);Tg(flk1:mCherry)* fish showed that the *spi2*-GFP<sup>+</sup> cells were restricted to the floor of the DA at 30 hpf (Fig. 2B). Time-lapse imaging further showed that the *spi2*-GFP<sup>+</sup> cells in the DA floor could undergo EHT (Fig. 2C), confirming their HEC identity. In parallel, we also outcrossed this reporter line with *Tg(gata1a:DsRed)* or *Tg(corola:DsRed)*

fish, where erythrocytes or leukocytes are marked by DsRed, respectively (Traver et al., 2003; Xu et al., 2015). Examination of these double transgenic lines showed that the *spi2*-GFP signals were detected in *gata1a:DsRed*<sup>+</sup> erythroid progenitors and *corola:DsRed*<sup>+</sup> leukocyte progenitors in the CHT at 3 dpf (Fig. 2D; Fig. S2A). These observations indicate that the *TgBAC(spi2:P2a-GFP)* reporter line recapitulates endogenous *spi2* expression.

To examine *spi2* expression in adult hematopoiesis, we analyzed the KM of adult *TgBAC(spi2:P2a-GFP)* zebrafish using fluorescence-activated cell sorting (FACS). Results showed that *spi2*-GFP<sup>+</sup> cells were predominantly detected in the myeloid (84.3±1.7%) and progenitor (HSPCs) (8.2±1.5%) populations (Fig. 2E). Similar observations were also found in the KM of adult *TgBAC(spi2:P2a-GFP);Tg(corola:DsRed)* double transgenic zebrafish, where GFP<sup>+</sup>DsRed<sup>+</sup> cells were found (98.1±1.8%) in the myeloid and HSPC populations (Fig. S2B,C). These observations suggest that *spi2* is predominantly expressed in HSPCs and myeloid lineages in adult hematopoiesis. To further support this conclusion, we isolated erythrocytes (*globin:eGFP*<sup>+</sup> cells), T cells (*lck:DsRed*<sup>+</sup> cells), thrombocytes (*cd41:eGFP*<sup>high</sup> cells), HSPCs (*cd41:eGFP*<sup>low</sup> cells) and myeloid cells (*pu.1:GFP*<sup>+</sup> cells) from adult KM to examine the expression of endogenous *spi2*. qPCR analysis revealed that *spi2* was detected exclusively in the *pu.1:GFP*<sup>+</sup> and *cd41:eGFP*<sup>+</sup> cells (Fig. 2F). Collectively, these data show that *spi2* expression is restricted to HSPCs, myeloid cells and thrombocytes in adult hematopoiesis.

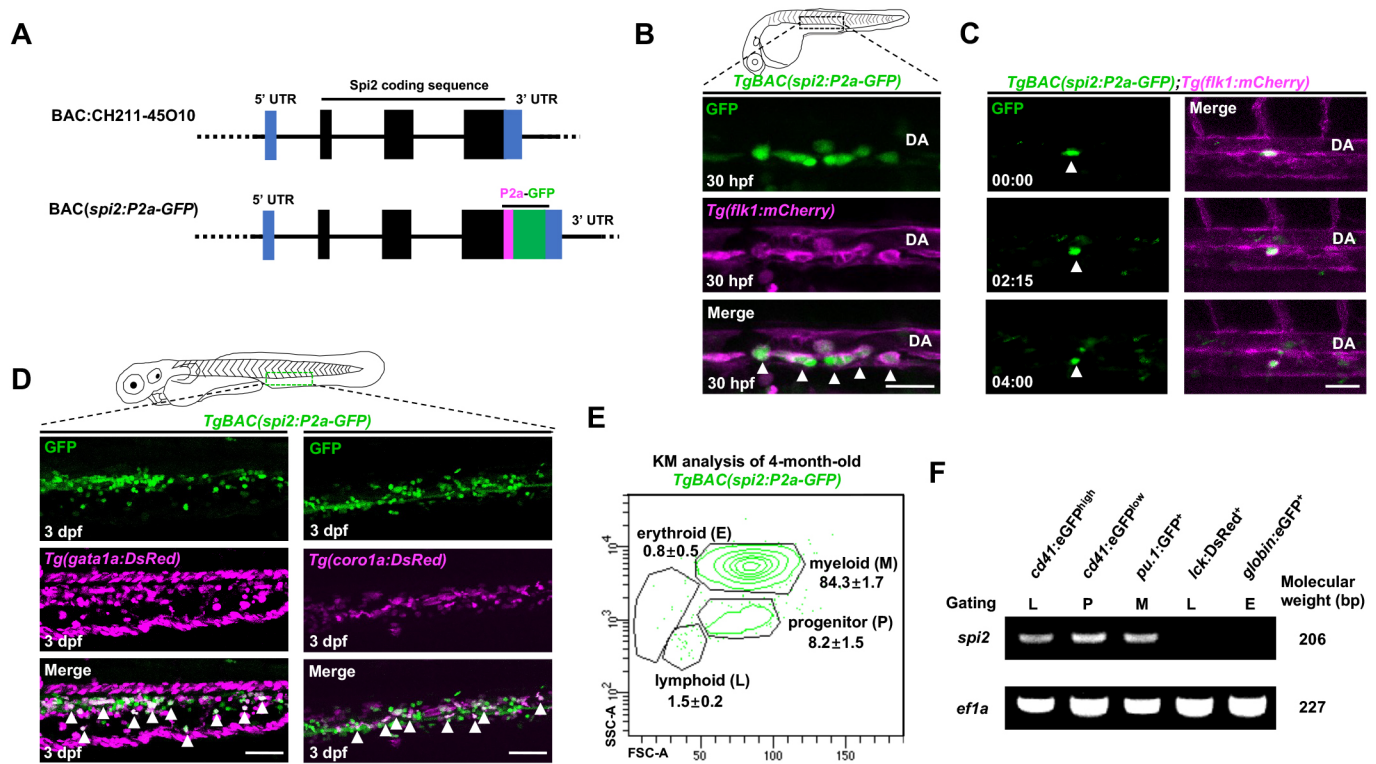


**Fig. 2. Generation and characterization of *TgBAC(spi2:P2a-GFP)* zebrafish.** (A) Strategy for generating *spi2* BAC construct. (B) Images of *spi2:GFP* expression in the aorta-gonad-mesonephros (AGM) in the *TgBAC(spi2:P2a-GFP);Tg(flk1:mCherry)* fish at 30 hpf. DA, dorsal aorta. Arrowheads show GFP<sup>+</sup>mCherry<sup>+</sup> cells. (C) Time-lapse imaging frames of *TgBAC(spi2:P2a-GFP);Tg(flk1:mCherry)* fish indicate an endothelial-to-hematopoietic transition (EHT) event of an *spi2-GFP*<sup>+</sup> cell (white arrowhead) from 30 hpf. (D) Images of the caudal hematopoietic tissue (CHT) in the *TgBAC(spi2:P2a-GFP);Tg(gata1a:DsRed)* (left) and *TgBAC(spi2:P2a-GFP);Tg(coro1a:DsRed)* (right) fish at 3 dpf. *spi2-GFP*<sup>+</sup> cells are co-localized with *gata1a-DsRed*<sup>+</sup> (left, white arrowhead) and *coro1a-DsRed*<sup>+</sup> (right, white arrowhead) cells. (E) FACS analysis of the kidney marrow (KM) of adult *TgBAC(spi2:P2a-GFP)* fish. *spi2-GFP*<sup>+</sup> cells are predominantly found in progenitor- and myeloid-gated populations. (F) qPCR analysis of *spi2* expression in FACS-gated populations from WT adult KM. *spi2* is enriched in HSPCs (*cd41:eGFP*<sup>low</sup>), myeloid cells (*pu.1-GFP*<sup>+</sup>), and thrombocytes (*cd41:eGFP*<sup>high</sup>). *ef1a* is used as an internal control. Scale bars: 30 μm (B); 40 μm (C); 60 μm (D).

### *spi2* deficiency impairs HSPC expansion during early development and myeloid development in adulthood

To explore the role of *spi2* in hematopoiesis, we generated a *spi2*-deficient mutant, in which 546 base pairs (bp) of the *spi2* genomic sequences were deleted (Fig. 3A), resulting in the synthesis of a truncated protein lacking the ETS domain (Fig. 3B). Further qPCR analysis showed that the truncated *spi2* transcripts were significantly reduced in *spi2* mutants (Fig. S3A), indicating that the *spi2* mutation is likely to be a null allele.

To dissect the role of *spi2* in hematopoiesis, we first examined the formation of embryonic erythroid and myeloid cells in *spi2*-deficient mutants at 22 hpf and 30 hpf. WISH showed that the expression of erythrocyte-marker *gata1a* (Rhodes et al., 2005), macrophage-marker *mfap4* (also known as *mfap4.1*) (Zakrzewska et al., 2010) and neutrophil-marker *lyz* (Hall et al., 2007) were all intact in *spi2* mutants (Fig. S3B,C), indicating that *spi2* is dispensable for primitive hematopoiesis. To explore the role of *spi2* in definitive hematopoiesis, we outcrossed *spi2* mutants with the *Tg(flk1:eGFP)* or *Tg(flk1:NLS-Eos)* fish, in which cECs and HECs are marked by GFP or NLS-Eos (Kissa and Herbomel, 2010; Zhao et al., 2022). Examination of the *Tg(flk1:eGFP)* transgenic zebrafish showed that the DA and HECs, as indicated by the GFP signal at 30 hpf and *runx1* WISH at 28 hpf, respectively, were intact in *spi2* mutants (Fig. 3C,D). Time-lapse imaging of *Tg(flk1:NLS-Eos)* transgenic zebrafish further revealed comparable EHT events in siblings (Movie 1) and *spi2* mutants (Fig. S3D; Movie 2),

indicating normal formation of HECs and HSPCs in *spi2*-deficient mutants. This conclusion was further validated by the FISH results showing that *c-myb*<sup>+</sup> (*myb*<sup>+</sup>) cells in the AGM were comparable between *spi2* mutants and siblings at 36 hpf (Fig. 3E,F). From 2 dpf onwards, however, the *c-myb*<sup>+</sup> cells in the CHT, where HSPCs are known to undergo rapid expansion (Murayama et al., 2006; Jin et al., 2007), in the mutant embryos were significantly reduced (Fig. 3E,F), suggesting that the maintenance of HSPCs in the CHT is impaired in *spi2* mutants. To further consolidate this conclusion, we outcrossed *spi2* mutants with the *Tg(cd41:eGFP)* zebrafish and quantified the number of *cd41:eGFP*<sup>low</sup> HSPCs (Kissa et al., 2008). Indeed, the number of the *cd41:eGFP*<sup>low</sup> cells in the CHT was markedly reduced in the mutants (Fig. S3E,F). Collectively, these observations demonstrate that *spi2* is dispensable for primitive hematopoiesis and the emergence of definitive HSPCs, but essential for the maintenance of definitive HSPCs in the CHT.

Previous studies have showed that definitive HSPCs are heterogeneous and are capable of differentiating into multiple lineages during early development (Jagannathan-Bogdan and Zon, 2013). To further define which hematopoietic lineages are impaired in *spi2* mutants during early development, we performed *hbae1* FISH (*hbae1.1*; erythrocytes), *rag1* FISH (T cells), anti-*lyz*:DsRed antibody staining (neutrophils) and anti-*mpeg1*:DsRed antibody staining (*mpeg1.1*; macrophages) at 5 dpf or 15 dpf when definitive hematopoietic lineages become predominant (He et al., 2018). Results showed that *spi2* mutants exhibited reduced neutrophils,

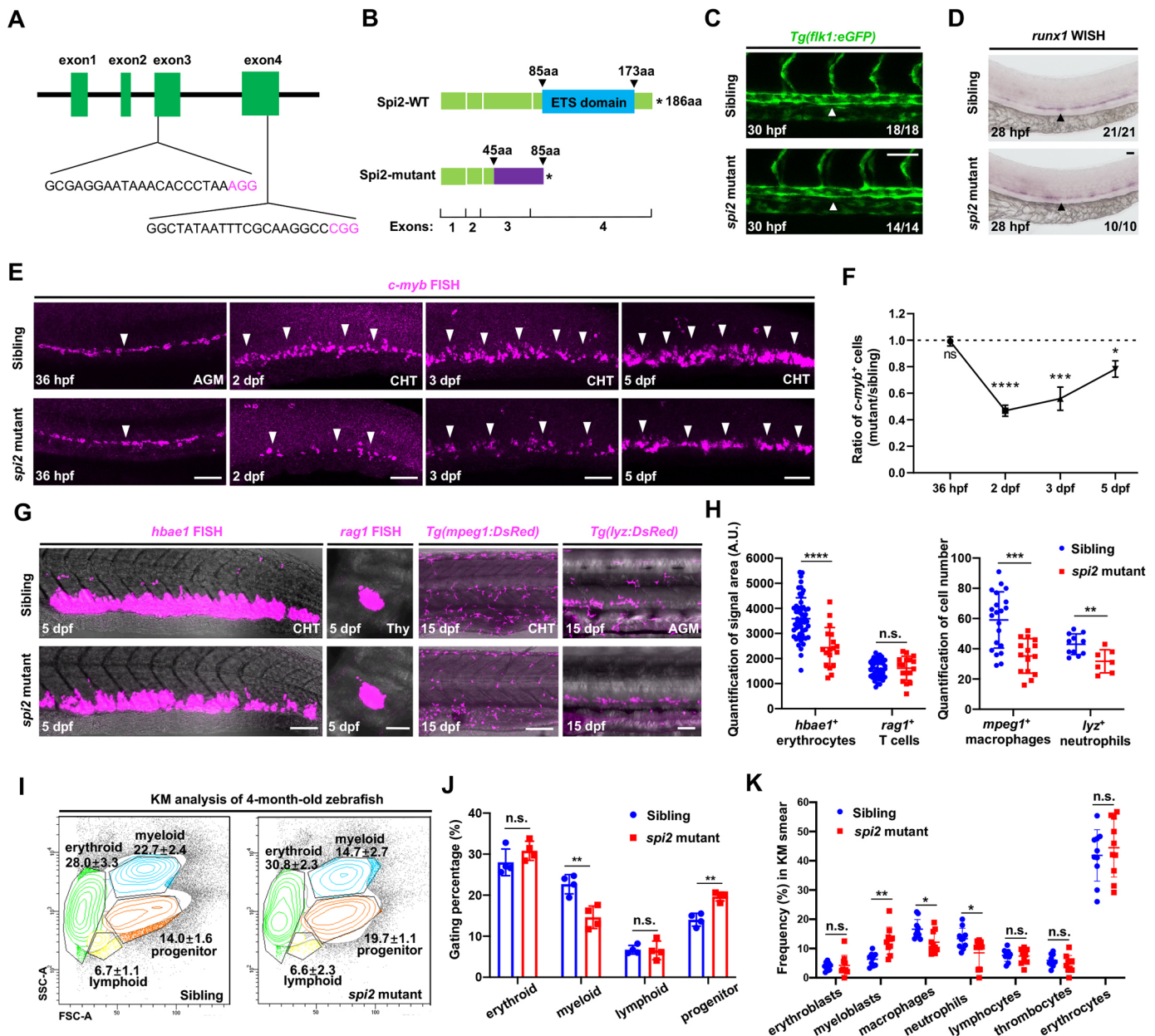


**Fig. 3.** *spi2* mutants are defective in HSPC maintenance in the CHT and myeloid cells in adulthood. (A) sgRNA design for generating *spi2* mutants. (B) The *spi2* mutation leads to a 546 bp deletion of the genomic sequences, resulting in generation of a truncated Spi2 protein lacking the ETS domain. (C) Images of *flk1*-eGFP expression indicating normal dorsal aorta (DA) formation in *spi2* mutants. White arrowheads show the vascular structure of the dorsal aorta (DA). (D) *runx1* WISH in *spi2* mutants and siblings in the aorta-gonad-mesonephros (AGM) at 28 hpf. Black arrowheads show *runx1*-expressing cells. (E) *c-myb* FISH in the AGM at 36 hpf and the caudal hematopoietic tissue (CHT) at 2 dpf, 3 dpf and 5 dpf in *spi2* mutants and siblings. White arrowheads show *c-myb*-expressing cells. (F) The ratio of *c-myb*<sup>+</sup> cells (the numbers of *c-myb*<sup>+</sup> cells in the mutants divided by the average number of *c-myb*<sup>+</sup> cells in siblings). Number of siblings or *spi2* mutants at 36 hpf, 2, 3 and 5 dpf: 47, 48, 23 and 20, or 18, 18, 10 and 13, respectively. (G,H) Images and quantification of *hbae1* FISH, *rag1* FISH, anti-*mpeg1*:DsRed<sup>+</sup> staining and anti-*lyz*:DsRed<sup>+</sup> staining in the AGM, CHT or thymus in *spi2* mutants and siblings at 5 dpf or 15 dpf. Numbers of siblings or *spi2* mutants: 55, 46, 21 and 11, or 18, 17, 15 and 7, respectively. (I,J) FACS analysis and quantification of the percentages of gated lineages in total singlet cells of whole KM in 5-month-old *spi2* mutants and siblings ( $n=4$  each). (K) MGG staining quantification of hematopoietic cell types in whole KM smear in 1-year-old *spi2* mutants and siblings ( $n=3$  each). Each dot indicates single captured image ( $n=10$  each). n/N reports the number of embryos with staining pattern in image/total embryos. Data are mean±s.d. n.s.,  $P > 0.05$ ; \* $P < 0.05$ ; \*\* $P < 0.01$ ; \*\*\* $P < 0.001$ ; \*\*\*\* $P < 0.0001$  (Unpaired Student's *t*-test). A.U., arbitrary unit. Scale bars: 60  $\mu$ m.

macrophages and erythrocytes, but normal T cells (Fig. 3G,H), indicating that *spi2*-deficiency predominantly affects erythroid and myeloid HSPCs during early embryogenesis.

As *spi2* transcripts are highly expressed in adult hematopoietic cells (Fig. 2E,F), we next investigated whether *spi2* deficiency would affect adult hematopoiesis. To address this issue, whole KM cells from adult *spi2* mutants and siblings were collected

and subjected to FACS analysis. We found that the myeloid lineage was significantly decreased in *spi2* mutants, accompanied by a moderate increase of progenitor population (Fig. 3I,J), showing that adult myelopoiesis is also impaired in *spi2* mutants. May-Grunwald-Giemsa (MGG) staining of whole KM cells further revealed that *spi2* mutants had reduced numbers of neutrophils and

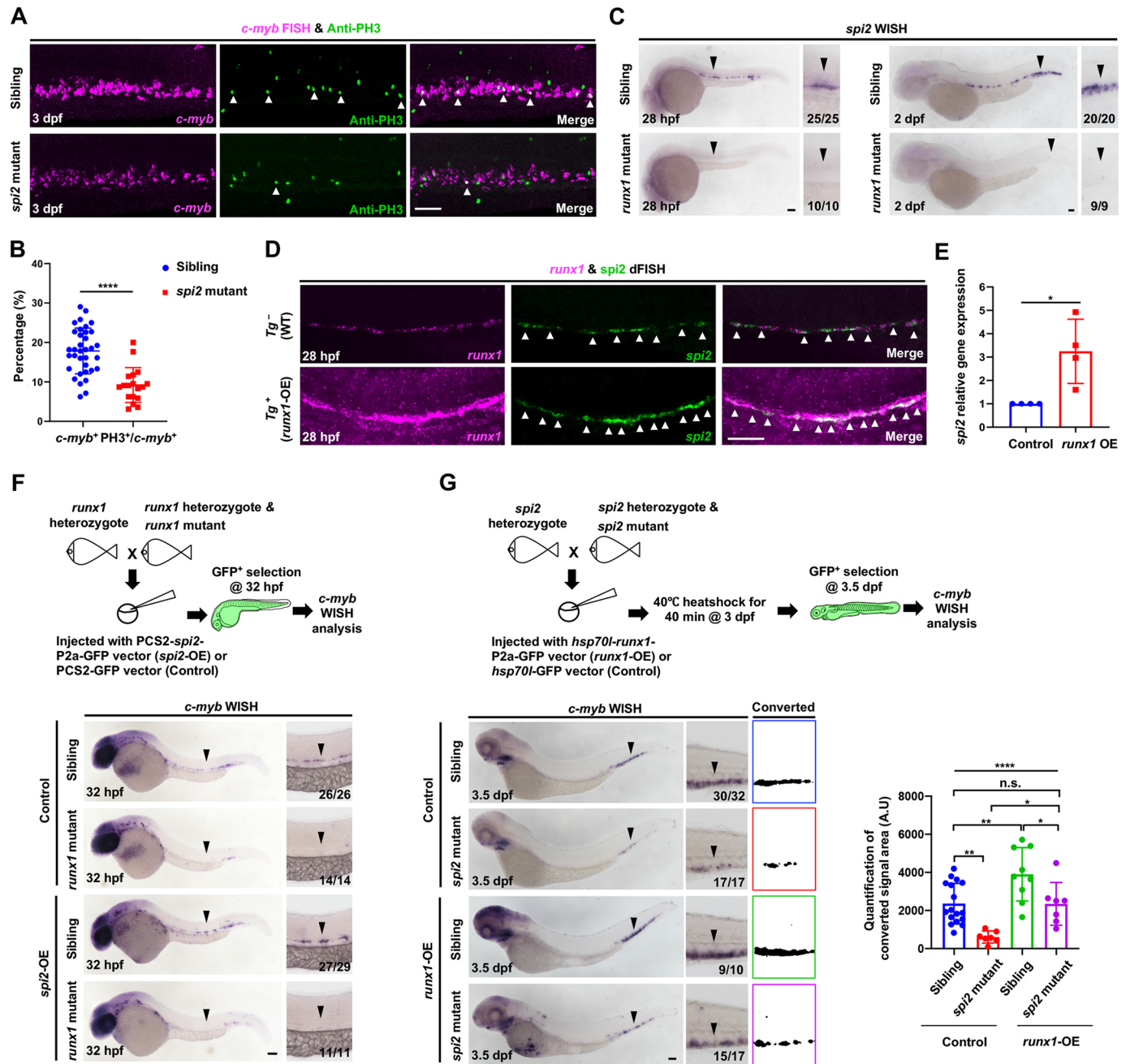


**Fig. 4. *spi2* acts downstream of *runx1* and regulates HSPC proliferation in the CHT.** (A) Images of *c-myb* FISH (magenta) and anti-PH3 staining (green) in the caudal hematopoietic tissue (CHT) in *spi2* mutants and siblings at 3 dpf. White arrowheads show *c-myb*<sup>+</sup>PH3<sup>+</sup> cells. (B) The percentage of *c-myb*<sup>+</sup>PH3<sup>+</sup> cells in the CHT in *spi2* mutants (*n*=18) and siblings (*n*=35) at 3 dpf in A. (C) WISH of *spi2* in the aorta-gonad-mesonephros (AGM) and CHT in *runx1*<sup>W84X</sup> mutants and siblings at 28 hpf and 2 dpf. Black arrowheads show *spi2*-expressing cells. (D) dFISH of *runx1* (magenta) and *spi2* (green) in the AGM of WT (Tg<sup>-</sup>) and *runx1*-overexpressed Tg(*flk1:runx1*-P2a-GFP) embryos (Tg<sup>+</sup>: *runx1*-OE) at 28 hpf. White arrowheads show *runx1*<sup>+</sup>*spi2*<sup>+</sup> cells. (E) qPCR analysis of *spi2* expression in *runx1*-OE and control endothelial cells (ECs). *runx1*-OE, ECs with *runx1* overexpression; Control, ECs without *runx1* overexpression. (F) *c-myb* WISH in 32 hpf *runx1* mutants and siblings with or without *spi2* overexpression. PCS2-*spi2*-P2a-GFP (*spi2*-OE) or PCS2-GFP (control) vector was injected into one-cell stage embryos. Black arrowheads show *c-myb*-expressing cells. (G) *c-myb* WISH and quantification of *c-myb* signals in the CHT in *spi2* mutants and siblings with (siblings *n*=17; mutants *n*=7) or without (siblings *n*=9; mutants *n*=7) *runx1* overexpression. *hsp70l*-*runx1*-P2a-GFP (*runx1*-OE) or *hsp70l*-GFP (control) vector was injected into one-cell stage embryos. Heat shock was performed at 3 dpf at 40°C for 40 min. Black arrowheads show *c-myb*-expressing cells. Data are mean±s.d. n.s., *P*>0.05; \**P*<0.05; \*\**P*<0.01; \*\*\*\**P*<0.0001. (An unpaired Student's *t*-test was used in B and E. Two-way analysis of variance (ANOVA), followed by Tukey's multiple comparisons tests were used in G.) Scale bars: 60 μm.

macrophages, accompanied by a higher number of undifferentiated myeloblasts (Fig. 3K; Fig. S3G), indicating that *spi2* is required for adult myeloid development, possibly at the stage of myeloblasts differentiating towards neutrophils and monocytes/macrophages.

### ***spi2* acts downstream of *runx1* to regulate HSPC proliferation in the CHT**

To delineate the cellular basis underlying the HSPC phenotype in *spi2* mutants, we performed terminal deoxynucleotidyl transferase dUTP nick-end labeling (TUNEL) assay and anti-phospho-histone 3 (PH3)

staining to monitor the cell death and proliferation of HSPCs in the CHT, respectively. TUNEL assay showed that the mutants and siblings had a comparable percentage of *c-myb*<sup>+</sup>TUNEL<sup>+</sup> HSPCs (Fig. S4A). In contrast, a significant decrease in the percentage of *c-myb*<sup>+</sup>PH3<sup>+</sup> HSPCs was observed in *spi2* mutants (Fig. 4A,B), indicating that the reduction of HSPCs in *spi2* mutants is largely attributed to the impaired proliferation of HSPCs in the CHT. Although the number of HSPCs in *spi2* mutants showed slight recovery by 5 dpf (Fig. 3F), the number of HSPCs in the mutants remained significantly lower than that in siblings (Fig. 3H), consistent with the continuously lower proliferative rate of HSPCs at 5 dpf in the mutants (Fig. S4B).

It is well-known that transcription factor Runx1 is essential for HEC fate specification, EHT and HSPC proliferation (Kissa and Herbomel, 2010; Eliades et al., 2016; Gao et al., 2018; Yzaguirre et al., 2018; Zhao et al., 2022). Double fluorescence *in situ* hybridization (dFISH) showed that *spi2* and *runx1* were largely overlapped in the floor of the DA (Fig. S4C). Based on the expression pattern of *spi2* and *runx1* (Bonkhofer et al., 2019) and the phenotype of *spi2*- and *runx1*-deficient mutants (Jin et al., 2009; Kissa and Herbomel, 2010), we speculated that *spi2* would likely be a downstream target of *runx1*. To elucidate the epistatic relationship between *spi2* and *runx1*, we probed the expression of *spi2* in *runx1* mutants (Jin et al., 2009) and showed that *spi2* was absent in *runx1* mutants (Fig. 4C), indicating that *spi2* acts downstream of *runx1*. To further support this conclusion, we took advantage of *Tg(flk1:runx1-P2a-GFP)* fish (Zhao et al., 2022), in which *runx1* expression is under control of the endothelial *flk1* promoter, to test whether overexpressing *runx1* could induce *spi2* expression. Indeed, increased *spi2* expression was observed in the floor of the DA in the *runx1*-overexpression embryos (Fig. 4D). To quantitatively compare the expression of *spi2* in *runx1*-overexpressed and control embryos, we crossed *Tg(flk1:mCherry)* with *Tg(flk1:runx1-P2a-GFP)* fish and sorted mCherry<sup>+</sup>GFP<sup>+</sup> (HECs and cECs with *runx1* overexpression) and mCherry<sup>+</sup>GFP<sup>-</sup> (HECs and cECs without *runx1* overexpression) cells from the trunk region of *Tg(flk1:mCherry);Tg(flk1:runx1-P2a-GFP)* or *Tg(flk1:mCherry)* embryos at 28 hpf, respectively (Fig. S4D). qPCR analysis revealed upregulated *spi2* expression in *runx1*-overexpressed mCherry<sup>+</sup>GFP<sup>+</sup> endothelial population (Fig. 4E), demonstrating that *spi2* indeed acts genetically downstream of *runx1*. However, forced expression of *spi2* failed to rescue the formation of HSPCs in *runx1* mutants as indicated by the lack of *c-myb*<sup>+</sup> cells in the AGM at 32 hpf (Fig. 4F), consistent with the finding that *spi2* is dispensable for HSPC emergence (Fig. 3E). To examine the role of *runx1-spi2* axis in HSPC expansion in the CHT, we overexpressed *runx1* by injecting the *hsp70l-runx1-P2a-GFP* DNA constructs into *spi2* mutants and siblings, and we found that overexpressing *runx1* led to a robust increase of *c-myb*<sup>+</sup> HSPCs in the CHT in siblings, but this increase was reduced in *spi2* mutants (Fig. 4G), suggesting that Spi2 works together with other Runx1 downstream factor(s) to regulate HSPC expansion in the CHT.

In conclusion, our study identified a previously uncharacterized ETS factor Spi2 in zebrafish and revealed its essential role in definitive hematopoiesis. Despite the lack of corresponding mammalian ortholog, Spi2 may take the partitioning function of Pu.1, a conserved master regulator of myeloid lineage development in fish and mammals (Scott et al., 1994; Burda et al., 2010; Yu et al., 2017). The specific expression of Spi2 in HECs and HSPCs and its role in HSPC maintenance indicate the adaptive neofunctionalization. It will be of interest to perform cross-species functional analysis of Spi2 to gain insights into the gene diversification.

## MATERIALS AND METHODS

### Zebrafish strains and maintenance

Zebrafish were maintained according to standard protocols (Westerfield, 2000). Embryos used for experiments were kept at 28.5°C in 0.5× E2 medium containing methylene blue (egg water) and changed to 0.003% N-Phenylthiourea (P7629, Sigma-Aldrich) egg water at 1 dpf to block pigmentation. The following strains were used: AB, *Tg(flk1:eGFP)s843* (Jin et al., 2005), *Tg(cd41:eGFP)* (Lin et al., 2005), *Tg(corola:DsRed)* (Xu et al., 2015), *Tg(gata1:DsRed)* (Traver et al., 2003), *Tg(globin:eGFP)* (Ganis et al., 2012), *Tg(lck:DsRed)* (Tian et al., 2017), *Tg(mpeg1:DsRed)* (He et al., 2018), *TgBAC(c-myb:GFP)* (Zhang et al., 2012), *Tg(flk1:runx1-P2a-GFP)hkz041* (Zhao et al., 2022), *Tg(flk1:NLS-Eos)ncv6* (Fukuhara et al., 2014), *TgBAC(spi2:P2a-GFP)hkz046* and *spi2<sup>hkz18</sup>*. This research was conducted according to the guidelines of the Animal and Plant Care Facility and approved by the Animal Ethics Committee of the Hong Kong University of Science and Technology.

### Generation of *spi2* mutant zebrafish

The *spi2* mutants were created using the CRISPR/Cas9 system (Chang et al., 2013). Briefly, two sgRNAs were designed using the CRISPR design tool (<http://www.e-crisp.org/E-CRISP/>) to target exon 3 (5'-3': GCGAGGAATAAACACCCTAAAGG) and exon 4 (5'-3': GGCTATAATTTTCGCAAGGCCCGG) of the *spi2* gene. The double strand DNA templates for *spi2* gRNAs synthesis were PCR amplified from the pMD-19-T-gRNA scaffold vector (Chang et al., 2013) (primers used for amplification: gRNA FP1: 5'-TAATACGACTCACTATAGGGCGAG-GAATAAACACCCTAAAGTTTGTAGAGCTAGAAATAGC-3'; gRNA FP2: 5'-TAATACGACTCACTATAGGGCTATAATTTTCGCAAGGCC-GTTTTAGAGCTAGAAATAGC-3'; gRNA RP: 5'-AGCACCGACT-CGGTGCCACT-3') and purified with the QIAquick PCR Purification Kit (28104, Qiagen). gRNAs were synthesized from the amplified double strand DNA templates using the MEGA-shortsript Kit (AM1354, Invitrogen) and purified using a MEGAclear Transcription Clean-Up Kit (AM1908, Invitrogen). Cas9 protein (20 μM, M0646M, New England Biolabs) and gRNAs (120 ng/μl) were co-injected into one-cell-stage wild-type (WT) embryos. The injected embryos were raised to adult and outcrossed with WT for mutation screening.

### BAC transgenesis

The BAC transgenic line *TgBAC(spi2:P2a-GFP)* was generated as previously described (Suster et al., 2011; Wu et al., 2020). The BAC clone CH211-45010 was purchased from CHORI-211 library (BACPAC Resources Center). The modified *spi2:P2a-GFP* BAC constructs were extracted from the DH10B using the Nucleobond BAC 100 Kit (740579, Macherey-Nagel) and injected (30 ng/μl) together with transposase mRNA (50 ng/μl) into one-cell-stage WT embryos. The injected embryos were raised to adults and outcrossed with WT for transgene screening.

### WISH and dFISH

WISH was performed as previously described (Tian et al., 2017). AP-conjugated anti-digoxigenin antibody (11093274910, Roche, 1:2000 diluted in blocking buffer) and BM purple (11442074001, Roche) were used as the antibody and substrate for color reaction. dFISH assay was performed as previously described (Lauter et al., 2011). POD-conjugated anti-fluorescein antibody (11426346910, Roche, 1:2000 diluted in blocking buffer), POD-conjugated anti-digoxigenin antibody (11207733910, Roche, 1:2000 diluted in blocking buffer) and TSA-Cy3 or TSA-FITC (NEL741001KT, PerkinElmer) were used for color reaction. The RNA probes were *in vitro* synthesized with T7 RNA polymerase (Promega) with dig-RNA-labeling mix (11277073910, Roche) or fluorescein-RNA-labeling mix (11685619910, Roche). The probes sequences are listed below: *runx1* probe (NM\_131603.3; 385-2069); *spi2* probe (XM\_009300320.3; 182-841); *hbae1* probe (NM\_182940.3; 1-504); *rag1* probe (NM\_131389.1; 1430-2949); *c-myb* probe (NM\_001309822.1; 192-3013). WISH images were captured by Stereo Discovery V20 microscope (Zeiss) with digital camera (DS-Ri2, Nikon). dFISH images were captured by SP8 confocal microscope (Leica) and analyzed by ImageJ (National Institutes of Health).

### Cell proliferation and apoptosis assay

For cell proliferation detection, the PH3 staining was performed after FISH. Anti-PH3 antibody (sc-56739, Santa Cruz Biotechnology, 1:500) and Alexa 555-anti-mouse antibody (A-31570, Invitrogen, 1:400) were used as primary and secondary antibody, respectively. For cell apoptosis detection, TUNEL assay was performed. In brief, embryos were fixed with 4% paraformaldehyde (PFA) overnight at 4°C and dehydrated with methanol at -20°C. Then, the embryos were rehydrated with phosphate-buffered saline plus 0.1% Tween-20 detergent (PBST) for 20 min. After rehydration, the embryos were permeabilized with 25 µg/ml proteinase K for 15 min at 21°C and incubated with 45 µl labeling solution plus 5 µl enzyme solution (In Situ Cell Death Detection Kit, Fluorescein, Roche) at 37°C for 2 h. The embryos were washed three times with phosphate-buffered saline plus 0.1% Tween-20 detergent (PBST) for 5 min each and the images were examined by SP8 confocal microscope (Leica).

### Trunk tissues and KM dissection, FACS and RT-qPCR

For embryonic trunk tissues dissection, embryos at 28 hpf stages were pooled together (each biological replicate with 60~100 embryos). The trunk tissues of embryos were dissected with a 27G needle and then homogenized by syringe with a 27G needle. The cell suspension was prepared as previously described (Wu et al., 2020) and subjected to FACS analysis (FACS Aria IIIu). For KM dissection in adulthood, the KM of adult fish was dissected and homogenized by grinding on a 40 µm nylon mesh in 5% fetal bovine serum (FBS) in phosphate-buffered saline (PBS) solution. The cell suspensions were then subjected to flow cytometry analysis. The cDNA was prepared from sorted cells (100~500 cells per well; two or four technical replicates per sample) and amplified by Smart-seq2 protocol (Picelli et al., 2014). Real-time (RT)-qPCR was performed to quantify the *spi2* transcripts. qPCR primers used in this study are: *spi2* (fwd: 5'-ACATCATCCAGTGGCTCTGT-3'; rev: 5'-GGCAGTGACTTGACACGCT-3'); *efla* (fwd: 5'-TACTTCTCAGGCTGACTGTG-3; rev: 5'-ATCTTCTTGATGTATGCGCT-3').

### Immunofluorescent antibody staining and MGG staining

Zebrafish at 15 dpf were anesthetized on ice and fixed in 4% PFA at 4°C for at least 1 day. After washing with PBS, fixed samples were dehydrated with methanol at -20°C. After rehydration, the fish were permeabilized with 25 µg/ml proteinase K for 20 min at 21°C and blocked with blocking buffer (5% FBS in PBST) for 1 h. The anti-DsRed primary antibody (632496, Clontech) was diluted (1:400) in blocking buffer, and Alexa Fluor 555 anti-rabbit antibody (A31572, Invitrogen, 1:400 diluted in blocking buffer) was used as secondary antibody. After staining, samples were washed with PBST and imaged using a Leica SP8 confocal microscope. For MGG staining, the dissected KM was homogenized by grinding on a 40 µm nylon mesh in 5% FBS-PBS solution. The cell suspensions were smeared onto the slides by cytopsin (Shandon, Thermo Fisher Scientific) and the slides were then air dried and subjected to MGG stain (Sigma-Aldrich), according to the manufacturer's instructions.

### Generation of expression constructs, microinjection and heat-shock treatment

To generate the PCS2-*spi2*-P2a-GFP construct, *spi2* full-length coding sequence was amplified from 2 dpf stage zebrafish embryo cDNA using primers (5'-3'): *spi2*-F, ATGACGGATCTCTGTGCAT; *spi2*-R, CGCTGCTTCTTTGACCACGCT. The P2a-GFP sequence was amplified from previous *flk1-runx1*-P2a-GFP construct (Zhao et al., 2022). The two types of PCR products were assembled into a PCS2+ vector, the sequence of which can be obtained from the Addgene website (<https://www.addgene.org/vector-database/2295/>). To generate the *hsp70l-runx1*-P2a-GFP construct, *runx1*-P2a-GFP sequence was amplified from *flk1-runx1*-P2a-GFP construct and cloned under *hsp70l* promoter (Halloran et al., 2000). The plasmids were injected into one-cell-stage embryos. For heat-shock experiments, embryos at 3 dpf were collected in a 50 ml Falcon tube containing 5 ml of E3 embryo medium and submerged in a 40°C water bath for 40 min.

### Photoconversion and time-lapse imaging

Photoconversion was performed as previously described (Zhao et al., 2022). For time-lapse imaging, the embryos were subsequently mounted in 1%

low-melting-point agarose in E3 embryo medium with 0.01% tricaine for anesthetization. Time-lapse imaging was carried out on an SP8 confocal microscope using a 20× objective (Leica). A heated microscope chamber (28.5°C) was used for recording time-lapse videos. Stacks were taken every 15 min with a step size of 3.0 to 5.0 µm. Confocal stacks and time-lapse videos were analyzed using ImageJ.

### RNA extraction and cDNA synthesis

Embryos were anesthetized on ice and homogenized in Buffer RLT (RNeasy Mini Kit, Qiagen) using needles and syringes. The RNA was extracted using the RNeasy Mini Kit (74104, Qiagen) and reverse-transcribed with Superscript IV VILO Master Mix (11756050, Invitrogen).

### Quantification and statistical analysis

All statistical analyses were performed using GraphPad Prism version 8. Paired or unpaired Student's *t*-tests were used to calculate the two-tailed *P*-value for comparisons. For multiple comparisons, significances were calculated using two-way analysis of variance (ANOVA), followed by Tukey's multiple comparisons test. Data are presented as mean±standard deviation (s.d.). Statistical significance is shown as follows: n.s., *P*>0.05; \**P*≤0.05; \*\**P*≤0.01; \*\*\**P*≤0.001; \*\*\*\**P*≤0.0001.

### Acknowledgements

We thank Dr Shuting Wu, Ms Kefan Cheng, Ms Thi Huong Trinh and Mr Liang Lou for their help in FACS analysis. We are grateful to Mr Shachuan Feng for the insightful discussion.

### Competing interests

The authors declare no competing or financial interests.

### Author contributions

Conceptualization: S.Z., A.Z., Z.W.; Methodology: S.Z., A.Z., H.Z.; Validation: A.Z., H.Z.; Formal analysis: S.Z., A.Z., H.Z., Z.W.; Investigation: S.Z., A.Z.; Data curation: S.Z., A.Z., H.Z.; Writing - original draft: S.Z.; Writing - review & editing: Z.W.; Supervision: Z.W.; Funding acquisition: Z.W.

### Funding

This work was supported by grants from the National Key Research and Development Program of China (2018YFA0800200), Major Program of Shenzhen Bay Laboratory (S201101002), the Research Grants Council, University Grants Committee of Hong Kong (16103920; 16101621; AoE/M-09/12; T13-605/18-W; T13-602/21-N), the Croucher Foundation (CF20SC01) and the Innovation and Technology Commission of Hong Kong (ITCPD/17-9).

### References

- Bertrand, J. Y., Kim, A. D., Teng, S. and Traver, D. (2008). CD41+ cmyb+ precursors colonize the zebrafish pronephros by a novel migration route to initiate adult hematopoiesis. *Development* **135**, 1853-1862. doi:10.1242/dev.015297
- Bertrand, J. Y., Chi, N. C., Santoso, B., Teng, S., Stainier, D. Y. and Traver, D. (2010). Haematopoietic stem cells derive directly from aortic endothelium during development. *Nature* **464**, 108-111. doi:10.1038/nature08738
- Boisset, J. C., van Cappellen, W., Andrieu-Soler, C., Galjart, N., Dzierzak, E. and Robin, C. (2010). In vivo imaging of haematopoietic cells emerging from the mouse aortic endothelium. *Nature* **464**, 116-120. doi:10.1038/nature08764
- Bonkhofner, F., Rispoli, R., Pinheiro, P., Krecsmarik, M., Schneider-Swales, J., Tsang, I. H. C., de Bruijn, M., Monteiro, R., Peterkin, T. and Patient, R. (2019). Blood stem cell-forming haemogenic endothelium in zebrafish derives from arterial endothelium. *Nat. Commun.* **10**, 3577. doi:10.1038/s41467-019-11423-2
- Burda, P., Laslo, P. and Stopka, T. (2010). The role of PU.1 and GATA-1 transcription factors during normal and leukemogenic hematopoiesis. *Leukemia* **24**, 1249-1257. doi:10.1038/leu.2010.104
- Chang, N., Sun, C., Gao, L., Zhu, D., Xu, X., Zhu, X., Xiong, J.-W. and Xi, J. J. (2013). Genome editing with RNA-guided Cas9 nuclease in zebrafish embryos. *Cell Res.* **23**, 465-472. doi:10.1038/cr.2013.45
- Eliades, A., Wareing, S., Marinopoulou, E., Fadlullah, M. Z. H., Patel, R., Grabarek, J. B., Plusa, B., Lacaud, G. and Kouskoff, V. (2016). The hemogenic competence of endothelial progenitors is restricted by Runx1 silencing during embryonic development. *Cell Rep.* **15**, 2185-2199. doi:10.1016/j.celrep.2016.05.001
- Force, A., Lynch, M., Pickett, F. B., Amores, A., Yan, Y. L. and Postlethwait, J. (1999). Preservation of duplicate genes by complementary, degenerative mutations. *Genetics* **151**, 1531-1545. doi:10.1093/genetics/151.4.1531

- Fukuhara, S., Zhang, J., Yuge, S., Ando, K., Wakayama, Y., Sakaue-Sawano, A., Miyawaki, A. and Mochizuki, N. (2014). Visualizing the cell-cycle progression of endothelial cells in zebrafish. *Dev. Biol.* **393**, 10-23. doi:10.1016/j.ydbio.2014.06.015
- Ganis, J. J., Hsia, N., Trompouki, E., de Jong, J. L., DiBiase, A., Lambert, J. S., Jia, Z., Sabo, P. J., Weaver, M., Sandstrom, R. et al. (2012). Zebrafish globin switching occurs in two developmental stages and is controlled by the LCR. *Dev. Biol.* **366**, 185-194. doi:10.1016/j.ydbio.2012.03.021
- Gao, L., Tober, J., Gao, P., Chen, C., Tan, K. and Speck, N. A. (2018). RUNX1 and the endothelial origin of blood. *Exp. Hematol.* **68**, 2-9. doi:10.1016/j.exphem.2018.10.009
- Hall, C., Flores, M. V., Storm, T., Crosier, K. and Crosier, P. (2007). The zebrafish lysozyme C promoter drives myeloid-specific expression in transgenic fish. *BMC Dev. Biol.* **7**, 42. doi:10.1186/1471-213X-7-42
- Halloran, M. C., Sato-Maeda, M., Warren, J. T., Su, F., Lele, Z., Krone, P. H., Kawada, J. Y. and Shoji, W. (2000). Laser-induced gene expression in specific cells of transgenic zebrafish. *Development* **127**, 1953-1960. doi:10.1242/dev.127.9.1953
- He, S., Chen, J., Jiang, Y., Wu, Y., Zhu, L., Jin, W., Zhao, C., Yu, T., Wang, T., Wu, S. et al. (2018). Adult zebrafish Langerhans cells arise from hematopoietic stem/progenitor cells. *Elife* **7**, e36131. doi:10.7554/eLife.36131
- Jagannathan-Bogdan, M. and Zon, L. I. (2013). Hematopoiesis. *Development* **140**, 2463-2467. doi:10.1242/dev.083147
- Jin, S. W., Beis, D., Mitchell, T., Chen, J. N. and Stainier, D. Y. (2005). Cellular and molecular analyses of vascular tube and lumen formation in zebrafish. *Development* **132**, 5199-5209. doi:10.1242/dev.02087
- Jin, H., Xu, J. and Wen, Z. (2007). Migratory path of definitive hematopoietic stem/progenitor cells during zebrafish development. *Blood* **109**, 5208-5214. doi:10.1182/blood-2007-01-069005
- Jin, H., Sood, R., Xu, J., Zhen, F., English, M. A., Liu, P. P. and Wen, Z. (2009). Definitive hematopoietic stem/progenitor cells manifest distinct differentiation output in the zebrafish VDA and PBI. *Development* **136**, 647-654. doi:10.1242/dev.029637
- Kissa, K. and Herbomel, P. (2010). Blood stem cells emerge from aortic endothelium by a novel type of cell transition. *Nature* **464**, 112-115. doi:10.1038/nature08761
- Kissa, K., Murayama, E., Zapata, A., Cortés, A., Perret, E., Machu, C. and Herbomel, P. (2008). Live imaging of emerging hematopoietic stem cells and early thymus colonization. *Blood* **111**, 1147-1156. doi:10.1182/blood-2007-07-099499
- Kohyama, M., Ise, W., Edelson, B. T., Wilker, P. R., Hildner, K., Mejia, C., Frazier, W. A., Murphy, T. L. and Murphy, K. M. (2009). Role for Spi-C in the development of red pulp macrophages and splenic iron homeostasis. *Nature* **457**, 318-321. doi:10.1038/nature07472
- Kondo, M., Wagers, A. J., Manz, M. G., Prohaska, S. S., Scherer, D. C., Beilhack, G. F., Shizuru, J. A. and Weissman, I. L. (2003). Biology of hematopoietic stem cells and progenitors: implications for clinical application. *Annu. Rev. Immunol.* **21**, 759-806. doi:10.1146/annurev.immunol.21.120601.141007
- Lauter, G., Söll, I. and Hauptmann, G. (2011). Two-color fluorescent in situ hybridization in the embryonic zebrafish brain using differential detection systems. *BMC Dev. Biol.* **11**, 43. doi:10.1186/1471-213X-11-43
- Lin, H.-F., Traver, D., Zhu, H., Dooley, K., Paw, B. H., Zon, L. I. and Handin, R. I. (2005). Analysis of thrombocyte development in CD41-GFP transgenic zebrafish. *Blood* **106**, 3803-3810. doi:10.1182/blood-2005-01-0179
- Liu, F. and Patient, R. (2008). Genome-wide analysis of the zebrafish ETS family identifies three genes required for hemangioblast differentiation or angiogenesis. *Circ. Res.* **103**, 1147-1154. doi:10.1161/CIRCRESAHA.108.179713
- Murayama, E., Kissa, K., Zapata, A., Mordelet, E., Briolat, V., Lin, H.-F., Handin, R. I. and Herbomel, P. (2006). Tracing hematopoietic precursor migration to successive hematopoietic organs during zebrafish development. *Immunity* **25**, 963-975. doi:10.1016/j.immuni.2006.10.015
- Picelli, S., Faridani, O. R., Björklund, Å. K., Winberg, G., Sagasser, S. and Sandberg, R. (2014). Full-length RNA-seq from single cells using Smart-seq2. *Nat. Protoc.* **9**, 171-181. doi:10.1038/nprot.2014.006
- Postlethwait, J. H., Woods, I. G., Ngo-Hazelett, P., Yan, Y.-L., Kelly, P. D., Chu, F., Huang, H., Hill-Force, A. and Talbot, W. S. (2000). Zebrafish comparative genomics and the origins of vertebrate chromosomes. *Genome Res.* **10**, 1890-1902. doi:10.1101/gr.164800
- Rhodes, J., Hagen, A., Hsu, K., Deng, M., Liu, T. X., Look, A. T. and Kanki, J. P. (2005). Interplay of pu.1 and gata1 determines myelo-erythroid progenitor cell fate in zebrafish. *Dev. Cell* **8**, 97-108. doi:10.1016/j.devcel.2004.11.014
- Scott, E. W., Simon, M. C., Anastasi, J. and Singh, H. (1994). Requirement of transcription factor Pu.1 in the development of multiple hematopoietic lineages. *Science* **265**, 1573-1577. doi:10.1126/science.8079170
- Sharrocks, A. D. (2001). The ETS-domain transcription factor family. *Nat. Rev. Mol. Cell Biol.* **2**, 827-837. doi:10.1038/35099076
- Sizemore, G. M., Pitarresi, J. R., Balakrishnan, S. and Ostrowski, M. C. (2017). The ETS family of oncogenic transcription factors in solid tumours. *Nat. Rev. Cancer* **17**, 337-351. doi:10.1038/nrc.2017.20
- Su, G. H., Chen, H. M., Muthusamy, N., Garrett-Sinha, L. A., Baunoch, D., Tenen, D. G. and Simon, M. C. (1997). Defective B cell receptor-mediated responses in mice lacking the Ets protein, Spi-B. *EMBO J.* **16**, 7118-7129. doi:10.1093/emboj/16.23.7118
- Sumanas, S. and Choi, K. (2016). ETS transcription factor ETV2/ER71/Etsrp in hematopoietic and vascular development. *Curr. Top. Dev. Biol.* **118**, 77-111. doi:10.1016/bs.ctdb.2016.01.005
- Suster, M. L., Abe, G., Schouw, A. and Kawakami, K. (2011). Transposon-mediated BAC transgenesis in zebrafish. *Nat. Protoc.* **6**, 1998-2021. doi:10.1038/nprot.2011.416
- Tian, Y., Xu, J., Feng, S., He, S., Zhao, S., Zhu, L., Jin, W., Dai, Y., Luo, L., Qu, J. Y. et al. (2017). The first wave of T lymphopoiesis in zebrafish arises from aorta endothelium independent of hematopoietic stem cells. *J. Exp. Med.* **214**, 3347-3360. doi:10.1084/jem.20170488
- Traver, D., Paw, B. H., Poss, K. D., Penberthy, W. T., Lin, S. and Zon, L. I. (2003). Transplantation and in vivo imaging of multilineage engraftment in zebrafish bloodless mutants. *Nat. Immunol.* **4**, 1238-1246. doi:10.1038/ni1007
- Westerfield, M. U. <https://books.google.com/hk/books?id=PngEACAAJ>. (2000). *The Zebrafish Book: A Guide for the Laboratory Use of Zebrafish (Danio Rerio)*. University of Oregon Press.
- Willis, S. N., Tellier, J., Liao, Y., Trezise, S., Light, A., O'Donnell, K., Garrett-Sinha, L. A., Shi, W., Tarlinton, D. M. and Nutt, S. L. (2017). Environmental sensing by mature B cells is controlled by the transcription factors PU.1 and SpiB. *Nat. Commun.* **8**, 1426. doi:10.1038/s41467-017-01605-1
- Wu, S., Nguyen, L. T. M., Pan, H., Hassan, S., Dai, Y., Xu, J. and Wen, Z. (2020). Two topologically and functionally distinct microglial populations in adult zebrafish. *Sci. Adv.* **6**, eabd1160. doi:10.1126/sciadv.abd1160
- Xu, J., Zhu, L., He, S., Wu, Y., Jin, W., Yu, T., Qu, J. Y. and Wen, Z. (2015). Temporal-spatial resolution fate mapping reveals distinct origins for embryonic and adult microglia in zebrafish. *Dev. Cell* **34**, 632-641. doi:10.1016/j.devcel.2015.08.018
- Yu, T., Guo, W., Tian, Y., Xu, J., Chen, J., Li, L. and Wen, Z. (2017). Distinct regulatory networks control the development of macrophages of different origins in zebrafish. *Blood* **129**, 509-519. doi:10.1182/blood-2016-07-727651
- Yzaguirre, A. D., Howell, E. D., Li, Y., Liu, Z. J. and Speck, N. A. (2018). Runx1 is sufficient for blood cell formation from non-hemogenic endothelial cells in vivo only during early embryogenesis. *Development* **145**, dev158162. doi:10.1242/dev.158162
- Zakrzewska, A., Cui, C., Stockhammer, O. W., Benard, E. L., Spaik, H. P. and Meijer, A. H. (2010). Macrophage-specific gene functions in Spi1-directed innate immunity. *Blood* **116**, e1-e11. doi:10.1182/blood-2010-01-262873
- Zhang, Y., Morimoto, K., Danilova, N., Zhang, B. and Lin, S. (2012). Zebrafish models for dyskeratosis congenita reveal critical roles of p53 activation contributing to hematopoietic defects through RNA processing. *PLoS One* **7**, e30188. doi:10.1371/journal.pone.0030188
- Zhao, S., Feng, S., Tian, Y. and Wen, Z. (2022). Hemogenic and aortic endothelium arise from a common hemogenic angioblast precursor and are specified by the Etv2 dosage. *Proc. Natl. Acad. Sci. USA* **119**, e2119051119. doi:10.1073/pnas.2119051119